Aalborg Universitet

AALBORG UNIVERSITY
DENMARK

A Grid-Connected Smart Extendable Structure for Hybrid Integration of Distributed Generations

Bizhani, H.; Noroozian, R.; Muyeen, S. M.; Techato, K.; Blaabjerg, F.

A Grid-Connected Smart Extendable Structure for Hybrid Integration of Distributed Generations

HAMED BIZHANI[1], (Student Member, IEEE), **REZA NOROOZIAN**[1], (Member, IEEE),
S. M. MUYEEN[2], (Senior Member, IEEE), **KUAANAN TECHATO**[3],
AND FREDE BLAABJERG[4], (Fellow, IEEE)

[1]Department of Electrical Engineering, Faculty of Engineering, University of Zanjan, Zanjan 45371–38791, Iran
[2]School of Electrical Engineering Computing and Mathematical Sciences, Curtin University, Perth, WA 6102, Australia
[3]Faculty of Environmental Management, Prince of Songkla University, Songkhla 90110, Thailand
[4]Department of Energy Technology, Aalborg University, 9220 Aalborg, Denmark

Corresponding author: Kuaanan Techato (kuaanan.t@psu.ac.th)

ABSTRACT In this paper, a novel grid-connected smart and plug-and-play type extendable structure named unified multiport power electronic converter (UMPEC) for hybrid integration of distributed generation (DG) systems is presented. The proposed structure contains two types of connector ports. The first one is a set of AC connectors, which can be easily used to connect different types and numbers of AC-based DGs along with grid and loads. The second one is a set of DC connectors, which can interface DC-based DGs and storage units. Compared with the conventional and recently invented multi-stage power electronic topologies, the proposed structure enjoys less number of power electronic components, compactness, and plug-and-play capability of integrating AC and DC-based DGs. Considering shared components between different ports and their imposed boundaries on the operation of the UMPEC, a modified sequential space vector modulation is addressed, which makes it possible to control different ports independently, without compromising with maximum power harnessing from individual sources, which is another salient feature of this work. The proposed structure operation and performance is verified using a three DC and two AC connectors version, where wind and photovoltaic systems are independently interfaced to the grid.

INDEX TERMS Distributed generations, maximum power point tracking, modified sequential space vector modulation, photovoltaic system, unified power electronic interface, wind turbine.

I. INTRODUCTION

Nowadays due to the rapid increase of the electrical energy consumption, the increased cost of the fossil fuel based conventional power generation, the environmental concerns, and cost reduction of renewable-based technologies, much attention has been attracted to the renewable energy based distributed generation (DG) systems [1]. Besides the many advantages of renewable-based DGs such as low installation and maintenance costs, carbon footprint reduction, high efficiency and electrical loss reduction, these DGs cannot be individually used due to their generated power uncertainty [2], [3]. Therefore, concurrent utilization of renewable-based DGs might be an effective approach to generate a programmable and reliable power [4]. However, depending on the type of DG (AC or DC), multi-stage individual power

The associate editor coordinating the review of this manuscript and approving it for publication was Weixing Li.

electronic topologies, as shown in Fig. 1(a), are required for their grid interconnections, which increase the cost, volume, and system loss as well as raising the complexity and compatibility issues [5], [6]. To overcome these issues, the integration of DC sources using multi-input DC-DC converters as shown in Fig. 1(b) with the red dotted area is performed in the literature [7]–[15], AC and DC-based hybrid integration of DGs using multi-stage DC-DC converters, which is shown in Fig. 1(b) with the green dotted area, is reported in [16]–[22], and a multiport power electronic interface concept for unifying the individual converters is introduced in [23] and [24].

In [7], a three-input boost converter with two unidirectional and one bidirectional input for integration of photovoltaic (PV), fuel cell (FC), and storage systems is addressed. With some modifications, an extendable multi-input DC-DC boost converter, which comprises of two bidirectional ports for interfacing an AC output and storage, has been reported
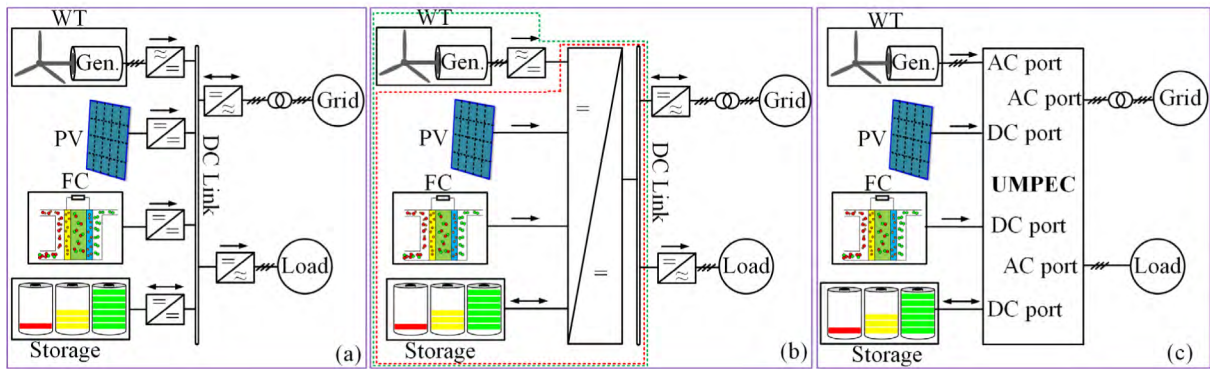
FIGURE 1. Different topologies for integration of DGs (a) Individual converter based, (b) Multi-input DC-DC converter based, and (c) Proposed topology.

in [8]. A dual-input high step-up DC-DC converter with zero voltage switching (ZVS) supplementary circuit, which is used for integration of two different PVs, is presented in [9]. A dual-input dual-buck inverter (DIDBI) with integrated boost converters (IBCs) for grid-connected applications is addressed in [10] in which two renewable-based DC sources, with independent operation conditions, can be integrated through the DIDBI and a constant and stable DC-link voltage is provided via IBCs. In [11], a multi-input converter based on three switches leg, which is able to integrate two or more similar DC inputs to an AC output is reported. A few three-port and multi-port converters for integration of the distributed generations are also reported in [12]–[15].

For grid integration of PV systems along with the wind turbines (WTs) different types of double input multi-stage DC-DC converters have been reported [16], [17]. The extracted power from the wind is first converted to the DC power through a diode rectifier. Then, by appropriate control of switches assigned to each input, PV and WT powers are transferred to the DC-link, and finally, this power is injected to the grid using a DC-AC inverter. The proposed structure reduces cost and is also able to track maximum power for both DGs, although, the WT experiences three stages of power conversion, which increases the system losses. A two-stage cascaded switched-diode (CSD) multilevel inverter for integration of the medium-voltage renewable energy sources along with the clock phase-shifting (CPS) one-cycle control (OCC) is addressed in [18]. A double-input isolated current-fed zero-current switching (ZCS) front-end DC-DC converter based multilevel inverter, which is able to integrates two renewable-based sources through two controllable switches is presented in [19]. In [20], a hybrid PV/WT/battery system is connected to the grid through an isolated multi-input DC-DC converter to inject a continuous power to the grid. In [21] and [22], the well-known nine-switch converter is used to integrate one AC and three DC sources. However, for grid connection an individual converter has been used. In order to unify all converters regardless of the connected source, the multi-input power electronic interfaces (MPEIs) concept is introduced [23]. In [23] and [24], the concept of MPEIs and procedure of

their modelling and design along with their dynamic behavior under load/source disturbances have been analyzed. A unified expandable power converter (UEPC), which is only able to integrate two or more AC-based DGs, is reported in [25].

In this study, in order to integrate both DC and AC-based DGs as well as reducing the number of switching components, a novel grid-connected smart plug-and-play extendable structure named unified multiport power electronic converter (UMPEC), which is shown in Fig. 1(c), is proposed. The proposed converter is an MPEI because it can integrate many DC and AC-based DGs. Besides, it is a unified structure because no individual converter is required for different inputs/outputs. The valid possible operation modes for proposed UMPEC are presented, and accordingly, a modified sequential space vector modulation (MSSVM) is developed to achieve independent control of different AC and DC ports. Finally, the performance of the proposed UMPEC and its MSSVM in hybrid integration of three photovoltaic systems along with one permanent magnet synchronous generator (PMSG) based wind turbine system are validated through a particular version of the proposed converter.

II. PROPOSED POWER CONVERTER TOPOLOGY AND OPERATION
A. THE TOPOLOGY OF THE PROPOSED UMPEC
The generalized version of the proposed UMPEC is shown in Fig. 2. As can be seen, the grid integration of both DC and AC sources can be only performed via a compact converter. Though all switches are common between all ports and it seems independent control of different ports is unachievable, but by using an appropriate switching method, this drawback can be avoided. In Fig. 2, DC-based DGs are connected to the lower ports, although, the grid and AC-based DGs are connected to the upper ports. It should be noticed that different sources might be placed in different positions. However, it makes the switching method difficult to be implemented. Therefore, in this paper, DC and AC sources are placed as shown in Fig. 2. Since for the integration of AC sources, bidirectional switches are required and due to the use of all switches in each leg to supply three-phase AC ports along
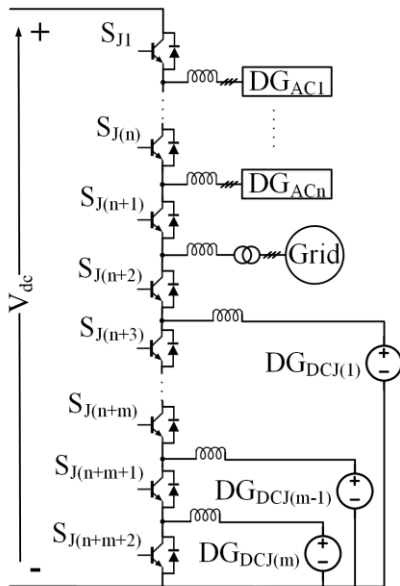
FIGURE 2. Generalized version of the proposed UMPEC topology integrating *n* AC based, *m* DC based DGs, and grid. J is A, B, and C.

TABLE 1. Comparison of conventional and proposed converters.

No. of DGs		No. of switches in different topologies	
AC based DGs	DC based DGs	Conventional Structure	Proposed Structure
1	1	14	10
2	1	20	13
3	1	26	16
1	2	16	11
1	3	18	12
⋮	⋮	⋮	⋮
n	*m*	$(6n+2m)+6$	$(3n+m)+6$

with DC-based DGs, all switches should be bidirectional. This means regardless of the type of the DC-based DGs (unidirectional or bidirectional), bidirectional power flow is available for all ports. Compared with the individual converter based topology for grid integration of *n* AC sources and *m* DC sources, as shown in Table 1, the proposed UMPEC requires $(3n + m)$ fewer switches. Furthermore, the advantages of the proposed UMPEC in comparison with recently invented topologies can be summarized as follows:

- The proposed UMPEC can integrate both DC and AC-based DGs. However, the presented converters in [7], [8], and [11]–[15] are only able to integrate the DC-based sources.
- In the proposed converter, grid interfacing is performed through a unified structure, which uses the same switching circuit as other AC ports, although an individual converter along with its switching circuit is required in [22].
- The unified converter reported in [25] can only be used for integration of AC-based DGs; however, the proposed UMPEC is capable of integrating both DC and AC-based DGs.
- The proposed UMPEC can significantly reduce the number of the power electronic switches compared to

23] and [24], which were using parallel configuration of the conventional DC-DC and DC-AC converters to create a unified structure.

B. PRINCIPLE OF OPERATION

As it is mentioned earlier, in the proposed UMPEC, all switches in each leg are shared between all AC and DC sources located in that leg. Therefore, the current of different sources passes through all switches, which means the operation modes of each port might be affected by others. To overcome this problem, in this paper, a modified sequential space vector modulation technique is developed to provide independent control of all ports. The DC-link voltage is regulated by grid side port and thus, each source might be autonomously controlled so that its operation in its maximum power point is guaranteed, which is explained in the following section.

III. PROPOSED MODIFIED SEQUENTIAL SPACE VECTOR MODULATION (MSSVM) TECHNIQUE FOR UMPEC

In sequential space vector modulation (SSVM), which has been used in [25] for independent control of AC outputs, the switching period is partitioned into $(n + 1)$ sub-periods according to the modulation index of each AC port. In each sub-period, the reference voltage of the corresponding AC port is constructed by switching of the active vectors of that port. At the same time, these active vectors generate zero vectors for the other AC ports. As it is indicated in Fig. 2, for grid integration of *n* AC and *m* DC sources (in each leg), which *m* can be different for different legs, $n+m+2$ switches are required in each leg. To avoid short-circuit in the DC-link, as shown in Table 2, $n + m + 1$ switches in each leg must be ON. Regarding this table and by removing the invalid status, individual active and zero vectors for different AC ports can be achieved as shown in Table 3, where *I* is the number of the AC port following the constraint $1 \leq I \leq n + 1$. It should be noticed that there might be some common active vectors between 2 to $n + 1$ AC ports, which can simultaneously be used to switch AC ports [25]. However, since the outputs can experience various conditions at different operating states, the probability of having the same voltage and frequency for different AC ports is low, which means the possibility of using the common vectors of all AC ports in the simultaneous switching is also low. These individual active vectors of each AC port make a space vector diagram for each port as shown in Fig. 3. The reference voltage of *I*-th AC port, which is generated by an individual controller, can be written as follows [25]:

$$V_{ref(I)} = \left| V_{ref(I)} \right| < \alpha_{(I)} \quad (1)$$

where

$$\alpha_{(I)} = 2\pi f_{(I)} t + \theta_{(I)} \quad (2)$$

where $f_{(I)}$ and $\theta_{(I)}$ are frequency and phase of *I*-th AC port. Firstly, to determine the switching signals, the sectors in which the reference vector of each AC port is located should

TABLE 2. ON and OFF switching states of each leg of the topology in fig. 2.

STATE No.	S_{J1}	S_{J2}	S_{J3}	...	$S_{J(K)}$	...	$S_{J(n)}$	$S_{J(n+1)}$	$S_{J(n+2)}$	$S_{J(n+3)}$	...	$S_{J(n+m)}$	$S_{J(n+m+1)}$	$S_{J(n+m+2)}$	
1	OFF	ON	ON	...	ON	...	ON	ON	ON	ON	...	ON	ON	ON	
2	ON	OFF	ON	...	ON	...	ON	ON	ON	ON	...	ON	ON	ON	
3	ON	ON	OFF	...	ON	...	ON	ON	ON	ON	...	ON	ON	ON	Active modes for grid and AC sources and charging mode for all DC sources located in J-th leg
:	:	:	:	...	:	...	:	:	:	:	...	:	:	:	
K	ON	ON	ON	...	OFF	...	ON	ON	ON	ON	...	ON	ON	ON	
:	:	:	:	...	:	...	:	:	:	:	...	:	:	:	
n	ON	ON	ON	...	ON	...	OFF	ON	ON	ON	...	ON	ON	ON	
n+1	ON	ON	ON	...	ON	...	ON	OFF	ON	ON	...	ON	ON	ON	
n+2	ON	ON	ON	...	ON	...	ON	ON	OFF	ON	...	ON	ON	ON	
n+3	ON	ON	ON	...	ON	...	ON	ON	ON	OFF	...	ON	ON	ON	Zero modes for grid and AC sources, charging mode for some DC sources, and discharging mode for others
:	:	:	:	...	:	...	:	:	:	:	...	:	:	:	
n+m	ON	ON	ON	...	ON	...	ON	ON	ON	ON	...	OFF	ON	ON	
n+m+1	ON	ON	ON	...	ON	...	ON	ON	ON	ON	...	ON	OFF	ON	
n+m+2	ON	ON	ON	...	ON	...	ON	ON	ON	ON	...	ON	ON	OFF	

TABLE 3. Individual active vectors of different AC ports of UMPEC.

Generated vector	A	B	C
(100)	I+1	I	I
(110)	I+1	I+1	I
(010)	I	I+1	I
(011)	I	I+1	I+1
(001)	I	I	I+1
(101)	I+1	I	I+1

$$(0,1,0) \quad (1,1,0)$$
$$\{I,(I+1),I\} \quad \{(I+1),(I+1),I\}$$

$$(0,1,1) \quad V_{ref(I)} \quad \alpha_{(I)} \quad (1,0,0)$$
$$\{I,(I+1),(I+1)\} \quad \{(I+1),I,I\}$$

$$(0,0,1) \quad (1,0,1)$$
$$\{I,I,(I+1)\} \quad \{(I+1),I,(I+1)\}$$

$$V_0 = [\{I,I,I\},\{(I+1),(I+1),(I+1)\}, \ldots , \{(I+j),(I+j),(I+j)\}]$$

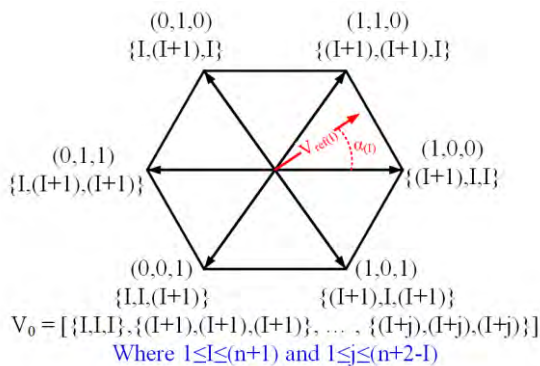Where $1 \leq I \leq (n+1)$ and $1 \leq j \leq (n+2-I)$

FIGURE 3. Space vector diagram of the I-th AC port in the proposed UMPEC.

be calculated. Then, the adjacent vectors of each reference vector must be identified, and finally the switching action is performed at a specific time for the each port. The time length assigned to each vector is calculated as follows:

$$T_{1(I)} = \sqrt{3}/2m_{(I)}T_s \sin\left(\left(k_{(I)}\right)\pi/3 - \alpha_{(I)}\right) \quad (3)$$

$$T_{2(I)} = \sqrt{3}/2m_{(I)}T_s \sin\left(\left(k_{(I)} - 1\right)\pi/3 - \alpha_{(I)}\right) \quad (4)$$

$$m_{(I)} = 2\left|V_{ref(I)}\right|/V_{dc} \quad (5)$$

where $T_{1(I)}$ and $T_{2(I)}$ are time intervals of the first and second adjacent active vectors of the I-th AC port, $m_{(I)}$ is the modulation index, $k_{(I)}$ is the identified sector for the I-th AC port, T_s is the switching period, and V_{dc} is the DC-link voltage.

To modify the SSVM in order to perform switching actions of the proposed UMPEC, which also contains DC sources along with AC sources, it is mandatory to understand the operation modes of AC and DC ports as well as the influences of the switching of the AC ports on DC sources and vice versa. By selecting various active vectors shown in Table 3, and applying related states shown in Table 2, the I-th AC port is in active mode, other AC ports are in zero mode, and all DC sources are in charging mode. Fig. 4 shows the operational modes and current flow of a particular version of UMPEC. As it can be seen, when active vectors for AC source and grid are applied (see Fig. 4(a) and (b)), all inductances connected to the DC sources are simultaneously charging. This means the fraction of the required time for charging the DC ports' inductances is filled while active vectors are being applied to the AC ports. It should be noticed that by applying zero vectors shown in Fig. 3 to the AC ports, DC sources experience the same situation (Fig. 4(c)). On the other hand, by turning one of the lowest switches off, as shown in Table 2, all AC ports are in zero state. Although as it is shown in Table 4, where J can be A, B, and C, depending on the position of that switch, some DC sources remaining in the charging mode and others are supposed to stay in discharging mode (See Fig. 4(d) to 4(f)).

In the proposed MSSVM, firstly, the adjacent active vectors of AC ports are sequentially applied similar to SSVM proposed in [25]. Then, according to the residue of the charging time of each DC source located in each leg, one of the states shown in Table 4 is selected.

IV. BOUNDARY CONDITIONS OF THE PROPOSED UMPEC

A. BOUNDARY CAUSED BY AC PORTS INFLUENCES

As it was mentioned earlier, while the active vectors are being applied to the AC ports, all DC sources are in charging mode, which means part of required charging mode for all DC sources are performed at the same time. Total time for applying active vectors to the AC ports can be written
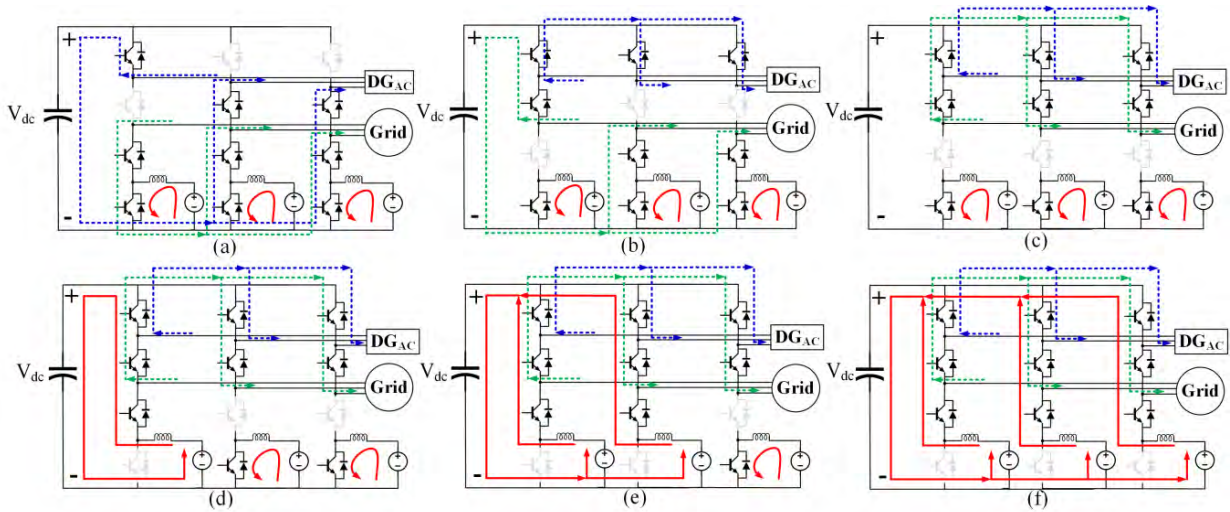
FIGURE 4. Operation modes and current flow for UMPEC where *n* = 1 and *m* = 3 (Each leg contains one DC source). (a) AC source is in active mode, (b) Grid is in active mode, (c) AC sources are in zero mode and DC sources are in charging mode (d) DC source 1 is in discharging mode, (e) DC source 1 and 2 are in discharging mode, and (f) all DC sources are in discharging mode.

TABLE 4. Charging and discharging modes for DC sources located in different legs.

Turned off switch in leg J	DC$_{J1}$	DC$_{J2}$	DC$_{J3}$	...	DC$_{J(m-1)}$	DC$_{J(m)}$
S$_{J(n+2)}$	CHARGE	CHARGE	CHARGE	...	CHARGE	CHARGE
S$_{J(n+2+1)}$	DISCHARGE	CHARGE	CHARGE	...	CHARGE	CHARGE
S$_{J(n+2+2)}$	DISCHARGE	DISCHARGE	CHARGE	...	CHARGE	CHARGE
⋮	⋮	⋮	⋮	...	⋮	⋮
S$_{J(n+2+m-1)}$	DISCHARGE	DISCHARGE	DISCHARGE	...	DISCHARGE	CHARGE
S$_{J(n+2+m)}$	DISCHARGE	DISCHARGE	DISCHARGE	...	DISCHARGE	DISCHARGE

as follow.

$$T_{\text{Active}} = \sum_{I=1}^{n+1} T_{1(I)} + T_{2(I)} \quad (6)$$

Therefore, as it is shown in Fig. 5, all DC sources experience an unavoidable charging mode for at least the period of T_{Active}, which imposes a boundary as follow:

$$T_{on}^{\min} \geq T_{Active} \Rightarrow D^{\min} \geq \frac{T_{Active}}{T_s} \quad (7)$$

where $T_{on}^{\min}$ and $D^{\min}$ are minimum acceptable time and duty cycle for charging mode of DC sources, respectively. By re-writing (6) the following is obtained:

$$T_{\text{Active}} = \sum_{I=1}^{n+1} \left(\sqrt{3}/2 m_{(I)} T_s \sin\left((k_{(I)}) \pi/3 - \alpha_{(I)} \right) \right. \\ \left. + \sqrt{3}/2 m_{(I)} T_s \sin\left((k_{(I)} - 1) \pi/3 - \alpha_{(I)} \right) \right) \quad (8)$$

This time will be maximum when:

$$\alpha_{(I)} = 2 \left(k_{(I)} - 1 \right) \pi/6 \quad (9)$$

By substituting (9) into (8) we have:

$$T_{\text{Actine}}^{\max} = (\sqrt{3}/2) \times T_s \sum_{I=1}^{n+1} m_{(I)} = \sqrt{3} \times T_s \sum_{I=1}^{n+1} V_{ref(I)}/V_{dc} \quad (10)$$

By substituting (10) into (7), the boundary can be written as follow:

$$D^{\min} \geq \sqrt{3} \sum_{I=1}^{n+1} V_{ref(I)}/V_{dc} \quad (11)$$

Considering the DC part of the proposed converter as a boost converter, $D^{\min}$ can be expressed as:

$$D^{\min} = \frac{V_{dc} - V_{DC}^{\max}}{V_{dc}} \quad (12)$$

where $V_{DC}^{\max}$ is the maximum voltage that might be connected to the DC ports of the UMPEC. By substituting (12) into (11), the exact value for this voltage can be written as follow:

$$V_{DC}^{\max} \leq V_{dc} - \sqrt{3} \sum_{I=1}^{n+1} V_{ref(I)} \quad (13)$$

From (13), the DC-link voltage and DC voltage sources should be selected in a way to satisfy this equation.

B. BOUNDARY CAUSED BY DC PORTS INTERACTION

In respect to Table 4 and Fig. 5, it is obvious that by turning the last switch in each leg off, all DC sources are supposed to experience discharging mode, which means the upper DC ports should have less charging mode compared with lower DC ports. To satisfy this boundary, the relation below should
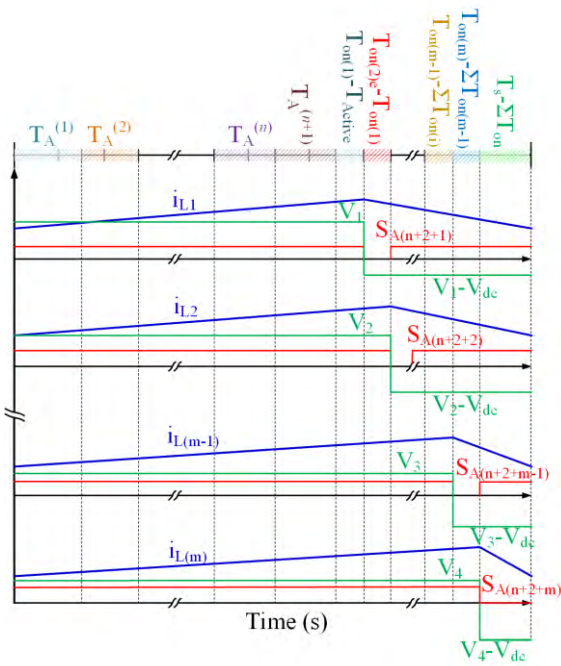
FIGURE 5. Steady-state waveforms of DC ports of the proposed converter in Fig. 2.

FIGURE 6. The current polarities of the sources.

TABLE 5. Instantaneous currents flowing through switches located in leg J for different switching states.

	S_{J1}=OFF	S_{J2}=OFF	S_{J3}=OFF	S_{J4}=OFF
i_{SJ1}	0	$-I_{AC}$	$-(I_{AC}-I_g)$	$-(I_{AC}-I_g+I_{DCJ})$
i_{SJ2}	I_{AC}	0	I_g	$-(I_{DCJ}-I_g)$
i_{SJ3}	$I_{AC}-I_g$	$-I_g$	0	$-I_{DCJ}$
i_{SJ4}	$I_{AC}-I_g+I_{DCJ}$	$-I_g+I_{DCJ}$	I_{DCJ}	0
Mode	Charging mode		Discharging mode	

be considered for design.

$$T_{on}^{(1)} \leq T_{on}^{(2)} \leq \ldots \leq T_{on}^{(m-1)} \leq T_{on}^{(m)} \qquad (14)$$

$$D^{(1)} \leq D^{(2)} \leq \ldots \leq D^{(m-1)} \leq D^{(m)} \qquad (15)$$

By substituting (12) into (15), the relation between DC sources of each leg can be written as follow:

$$V_{DC}^{(1)} \geq V_{DC}^{(2)} \geq \ldots \geq V_{DC}^{(m-1)} \geq V_{DC}^{(m)} \qquad (16)$$

It means open circuit voltages of DC sources in each leg should be designed in a way that the upper sources have higher voltages compared with the lower ones.

V. INSTANTANEOUS SWITCH CURRENTS

Due to the flowing of DC and AC ports currents through all switches located in each leg, the instantaneous switch currents, which are strongly related to the switching loss, should be examined explicitly. For this purpose, a specific version of the proposed topology shown in Fig. 4, which integrates an AC and three DC sources to the grid, is considered. Considering the current polarities as shown in Fig. 6, the instantaneous currents flowing through the switches can be summarized as Table 5. As it can be seen, since the AC and DC sources currents should pass through all switches in the first and last states, the upper and lower switches experience higher instantaneous currents, which might yield a higher switching loss. However, according to [21], [26], [27], in comparison to the unified power electronic converter presented in [25] for the integration of AC sources, the switching loss of the proposed topology might be lower depending on the phase and frequency of the grid side current along with the proportion
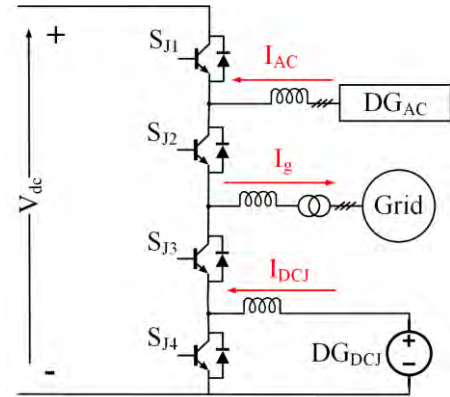
of I_g and I_{DCJ}. In other words, the combination of AC and DC sources ports creates an AC-DC different frequency mode in which according to [26], the switching loss can be lower.

VI. INDEPENDENT CONTROL OF DIFFERENT PORTS

Due to the capability of the proposed MSSVM applied to the developed UMPEC, the autonomous control of different ports are achievable. Depending on the type of AC ports, various controllers can be implemented. In this paper, to show the capability of the proposed converter in a hybrid integration of AC and DC-based DGs as well as autonomous control of them, the PMSG based variable speed wind turbines (VSWTs) along with PV systems are taken into consideration for AC ports and DC ports, respectively. Also, the last AC port is used as grid side converter, which is responsible for DC-link voltage regulation. The control details of AC and DC ports along with the DC-link voltage regulation is presented in the following sub-sections.

A. CONTROL OF AC SOURCES

In conventional PMSG based VSWTs, the generator side converter is responsible to control the mechanical speed of the rotor in order to capture maximum power from the wind. This task is properly done by using a maximum power point tracking (MPPT) controller as shown in Fig. 7 with the red dotted line. For this purpose, it is crucial to find the relation between the maximum captured power and mechanical speed in terms of wind speed. The mathematical relation for the extracted mechanical power from the wind can be expressed
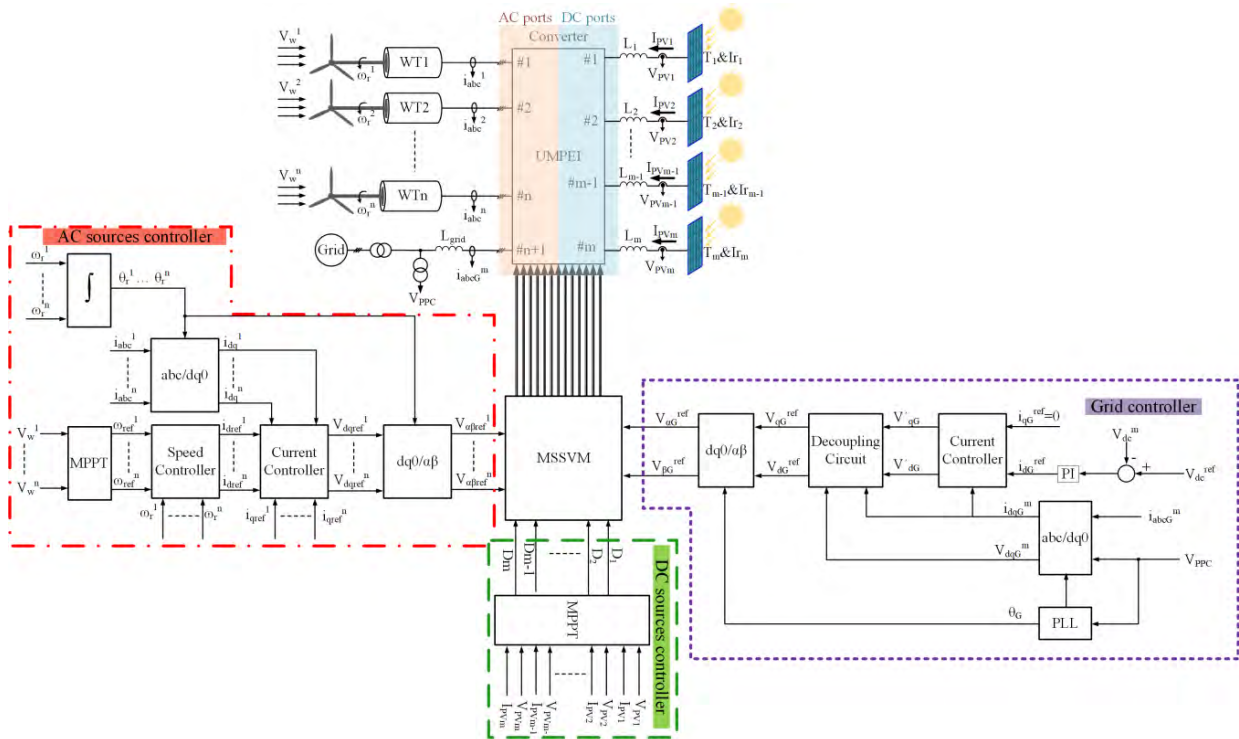
FIGURE 7. Control block diagram of the proposed converter with *n* numbers of wind turbines (as AC sources), *m* numbers of PVs (as DC sources), and grid.

as follow [25], [28]:

$$P_w = 0.5\rho\pi R^2 V_w^3 C_P(\lambda, \beta) \tag{17}$$

where P_w is the captured power from the wind, ρ is the air density $[kg/m^3]$, R is the blade radius $[m]$, V_w is the wind speed $[m/s]$ and C_p is the power coefficient, which is a function of both tip speed ratio, λ, and blade pitch angle, β $[deg]$. The tip speed ratio and C_p can be written as follows:

$$\lambda = \frac{\omega_r R}{V_w} \tag{18}$$

$$C_p = 0.73\left(\frac{151}{\lambda_i} - 0.58\beta - 0.002\beta^{2.14} - 13.2\right)e^{-18.4/\lambda_i} \tag{19}$$

where

$$\lambda_i = \left(\frac{1}{\lambda - 0.02\beta} + \frac{0.003}{\beta^3 + 1}\right)^{-1} \tag{20}$$

The pitch angle is only controlled when rotor speed exceeds the rated speed. Otherwise, it is kept constant at zero. In this paper, the operating conditions under the rated wind speed are considered therefore this value is zero. The maximum power that can be extracted from the wind can be rewritten as:

$$P_{w,\max} = 0.5\rho\pi R^2\left(\frac{R}{\lambda_{opt}}\right)^3 C_{p,\max}\omega_{r,opt}^3 = K_{opt}\omega_{r,opt}^3 \tag{21}$$

Initially, considering (18) and (24), the optimum speed for maximization of the captured power is calculated. Then,

using a speed controller the desired value for d-axis current, which is responsible for active power control, is determined. At the same time, for minimization of losses, the reference value for q-axis current is considered zero. Finally, using a well-designed current controller, the output reference voltages are achieved.

B. CONTROL OF DC SOURCES

The typical grid-connected PV system includes two converters. The first one, which is a DC-DC boost converter, is responsible for tracking the maximum power point according to weather conditions. The second one, which is a DC-AC converter, is responsible to regulate the DC-link voltage through the injecting generated active power to the grid. In the proposed UMPEC, the grid side converter is shared between AC and DC sources, which means no individual DC-AC converter is required for PV sources. Therefore, a proper MPPT controller for each PV as it is shown in Fig. 7 with the green dotted line is only needed. For this aim, a simple perturb and observe (P&O), which is being frequently used in the literature [16], is implemented. For a useful analysis of the DC connectors, the irradiation and temperature conditions of PV systems are considered diversely. It is noted that the calculated duty cycles of the DC sources located in each leg should have a relationship so that (15) meets in all time. Nevertheless, in this paper, three PV sources are located on different legs, which means the MPPT of the individual sources can work independently.
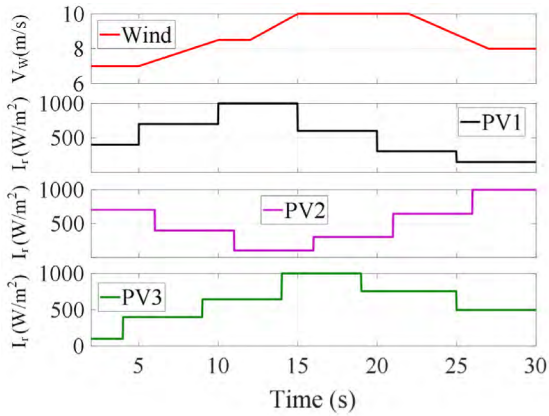
FIGURE 8. Applied test conditions to AC and DC-based DGs at variable wind speed and solar irradiance.

FIGURE 9. Simulation results, (a) rotational speed of turbine, and (b) tip speed ratio.

C. DC-LINK VOLTAGE REGULATION

In order to control the MPPT of the AC and DC sources appropriately, the DC-link voltage should be properly regulated. This purpose is achieved by effective control of the grid side AC port, which is the last AC port in the UMPEC, as shown in Fig. 7. For this purpose, using the same approach as [25], the DC-link voltage controller has been implemented in the synchronous frame, which is synchronized with grid side frequency. The d-axis current is used for DC-link voltage regulation although q-axis current might be used for reactive power control. However, in this paper, unity power factor at the grid side is the main aim and therefore, the reference value for q-axis current is zero.

VII. RESULTS AND VALIDATION

A. SCENARIO 1: THE NUMBER OF DC BASED DGS IS A MULTIPLE OF THREE

In order to validate the performance of the proposed structure for grid integration of the AC and DC sources and the effectiveness of the MSSVM, a particular version of UMPEC shown in Fig. 4, including two AC sources (PMSG based VSWT and main grid) and three DC sources (PV systems with different weather conditions), has been considered. The irradiation patterns for different PVs along with the wind speed pattern for the wind turbine are shown in Fig. 8. The tip speed ratio and mechanical speed of the wind turbine are shown in Fig. 9. As it can be seen, by appropriate control of the generator side converter shown in Fig. 7, the mechanical speed is coinciding with the optimum value calculated by the MPPT. As a result, regardless of the wind speed, the tip speed ratio will be matched with its optimum value, which means the maximum power is being perfectly captured from the wind. The generated power by PMSG and PVs are shown in Fig. 10. As can be seen, the variation in the generated power by DGs are similar to the applied conditions as shown in Fig. 8. The total generated power by DGs along with injected power to the grid is depicted in Fig. 11. As expected, the total power generated by DGs is equal to injected power
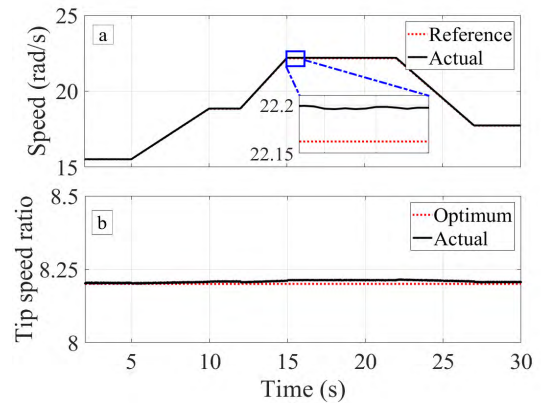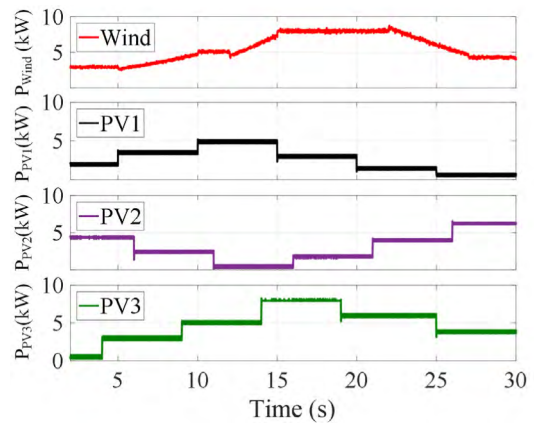

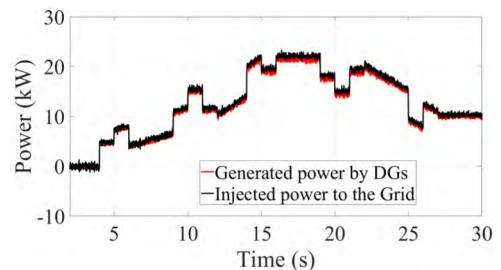**FIGURE 10.** Generated power by DGs.

FIGURE 11. Total generated power by DGs and injected power to the grid.

to the grid. Since the power flow between the sources is controlled by the grid and through the regulation of the DC-link voltage, it is expected to have a stable DC-link voltage, as shown in Fig. 12. The three-phase currents of the grid and their Fast Fourier Transform (FFT) spectrum are illustrated in Fig. 13. As can be seen, due to the using an effective modulation, the total harmonic distortion (THD) of the grid side current is within an acceptable range. As it is mentioned earlier, in order to have unity power factor in the grid side, the reference value for the q-axis current of the grid side controller has been set to zero, which means the injected reactive power to the grid, as shown in Fig. 14, should be zero. The current waveforms of the different inductances
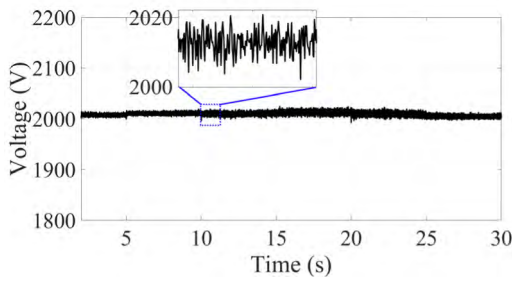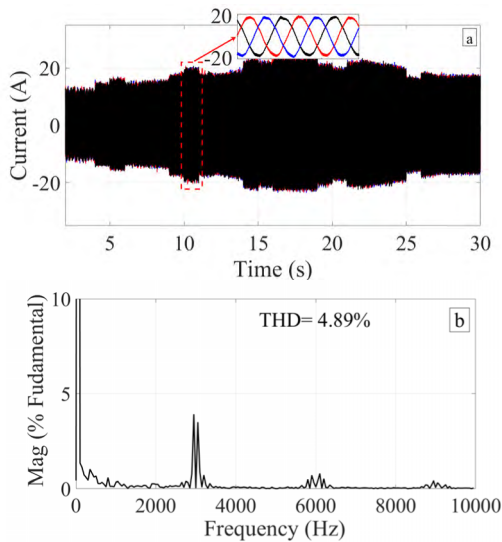
FIGURE 12. DC-link voltage.

FIGURE 13. Power quality responses, (a) Grid side three-phase currents, and (b) its FFT spectrum.
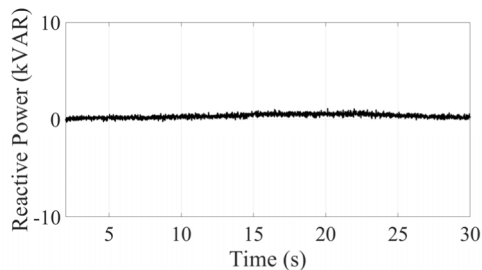

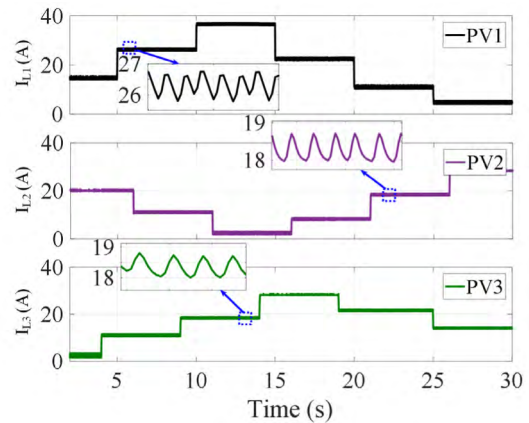FIGURE 14. Injected reactive power into the grid.

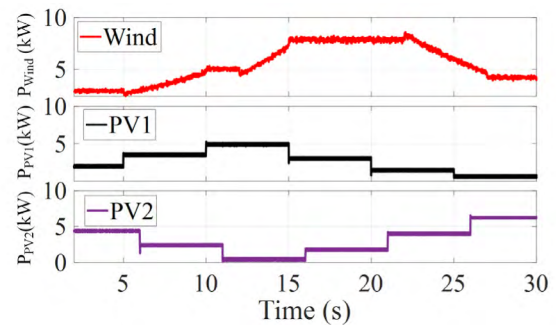FIGURE 15. Inductor currents of different DC sources (PVs).

FIGURE 16. Generated power by DGs in second scenario.

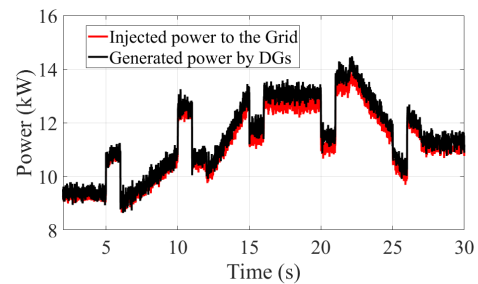FIGURE 17. Total generated power by DGs and injected power into the grid in second scenario.

located in DC ports, are depicted in Fig. 15. Due to a proportional relation between output current of PVs and applied irradiation, currents in the inductors changes according to the irradiation. By magnifying these currents as shown in Fig. 15, charging and discharging modes for different ports can be seen.

B. SCENARIO 2: THE NUMBER OF DC BASED DGS IS NOT A MULTIPE OF THREE
In order to show the capability of the proposed converter in handling asymmetrical distribution of DC-based DGs between the legs, one of the PV sources in the previous scenario is disconnected, which means only two PV sources

connected to leg A and B are integrated. In this case, as the third PV is disconnected, there is no need to turn the related switch OFF (which is the fourth switch in leg C). This aim will be achievable when the duty cycle of the disconnected PV in MSSVM is one. It should be noticed that in the design stage, as mentioned earlier and considering Fig. 2, the number of switches in each leg is determined according to the number of integrated DC-based DGs in each leg. For instance, if the number of DC-based DGs are two, leg A and B should contain four switches, although leg C might have three switches. Therefore, there is no fourth switch in leg C and hence there is no need to control it, which means the control of the switches related to DC sources located in leg A and B is only required.
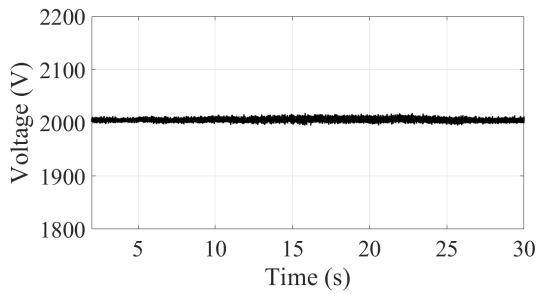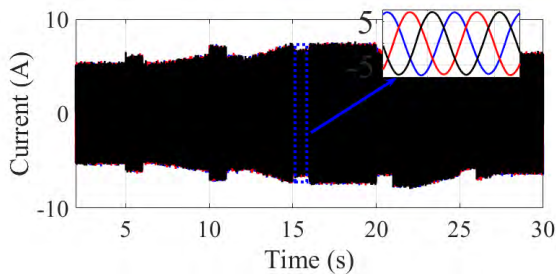
FIGURE 18. DC-link voltage in second scenario.

FIGURE 19. Grid-side current in second scenario.
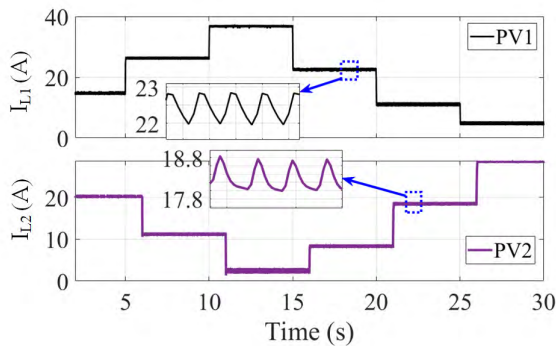

FIGURE 20. Inductor currents of different DC sources (PVs) in second scenario.

In order to provide the possibility of the comparison of the results with the previous scenario, the same test conditions are applied to the AC and DC sources. As it is shown in Fig. 16, the generated power by DGs follow the wind and irradiation patterns. It also can be seen that disconnecting of one of the DC-based DGs has no effect on the operation of the rest of system, which means regardless of the number of DC-based DGs, the appropriate operation of the proposed converter is guaranteed. Total generated power by AC and DC sources along with injected power to the grid are demonstrated in Fig. 17. As it is shown, the power flow between sources and grid is being satisfactorily done. According to DC link voltage shown in Fig. 18, this appropriate power flow can be also confirmed. With respect to Fig. 19, it can be deduced that despite the asymmetrical connection of DC sources between legs, the grid side current is not affected and as a result, this current stays symmetric. Inductor currents of PV sources are shown in Fig. 20. As it can be deduced,

disconnecting of one of the DC sources has no influence on other DC sources performance.

VIII. CONCLUSION

In this paper, a new approach for grid integration of the AC and DC-based distributed generation systems is demonstrated using a UMPEC. Unlike the conventional structures, which use individual/multi-stage converters for this aim, the proposed converter uses a unified smart plug-and-play structure, which can easily be extended to integrate more number of DGs. Due to the shared switches between AC and DC sources located in each leg, the performance of the different ports can be affected by others. In order to understand how these influences are, the principle of operation modes of the UMPEC is explicitly addressed. Then, a modified sequential space vector modulation, which can be generalized to be used for different versions of the UMPEC, is presented. It is revealed that without any overlap caused by using a unified structure between different ports, each port can be independently controlled, which means all renewable sources can successfully trace their maximum power points. In addition, the power flow between sources and grid is controllable through the DC-link voltage regulation performed by the AC port connected to the main grid. A particular version of the proposed converter, which is capable to integrate the grid, one PMSG based VSWT, and three PV systems at different weather conditions, is used to validate the performance of the UMPEC and its MSSVM. The results confirm the capability of the proposed topology in handling both symmetrical and asymmetrical distribution of DC sources between the legs. Compared with the traditional topologies, the proposed UMPEC can reduce the number of the required switching devices from 18 to 12, which yields to have a 33.3 % installation cost-effectiveness. This lower installation cost along with the effective performance of the proposed UMPEC make it an interesting alternative approach for hybrid integration of AC and DC based-DGs.

REFERENCES

[1] M. S. S. Abad, J. Ma, D. Zhang, A. S. Ahmadyar, and H. Marzooghi, "Probabilistic assessment of hosting capacity in radial distribution systems," *IEEE Trans. Sustain. Energy*, vol. 9, no. 4, pp. 1935–1947, Oct. 2018.

[2] J. Yan, F. Li, Y. Liu, and C. Gu, "Novel cost model for balancing wind power forecasting uncertainty," *IEEE Trans. Energy Convers.*, vol. 32, no. 1, pp. 318–329, Mar. 2017.

[3] K. Rahbar, C. C. Chai, and R. Zhang, "Energy cooperation optimization in microgrids with renewable energy integration," *IEEE Trans. Smart Grid*, vol. 9, no. 2, pp. 1482–1493, Mar. 2018.

[4] H. Ji, C. Wang, P. Li, F. Ding, and J. Wu, "Robust operation of soft open points in active distribution networks with high penetration of photovoltaic integration," *IEEE Trans. Sustain. Energy*, vol. 10, no. 1, pp. 280–289, Jan. 2019.

[5] A. Francés, R. Asensi, Ó. García, R. Prieto, and J. Uceda, "Modeling electronic power converters in smart DC microgrids—An overview," *IEEE Trans. Smart Grid*, vol. 9, no. 6, pp. 6274–6287, Nov. 2018.

[6] Z. Wang, W. Wu, and B. Zhang, "A distributed control method with minimum generation cost for DC microgrids," *IEEE Trans. Energy Convers.*, vol. 31, no. 4, pp. 1462–1470, Dec. 2016.

[7] F. Nejabatkhah, S. Danyali, S. H. Hosseini, M. Sabahi, and S. M. Niapour, "Modeling and control of a new three-input DC–DC boost converter for hybrid PV/FC/battery power system," *IEEE Trans. Power Electron.*, vol. 27, no. 5, pp. 2309–2324, May 2012.

[8] S. Danyali, S. H. Hosseini, and G. B. Gharehpetian, "New extendable single-stage multi-input DC–DC/AC boost converter," *IEEE Trans. Power Electron.*, vol. 29, no. 2, pp. 775–788, Feb. 2014.

[9] B. Zhu, Q. Zeng, Y. Chen, Y. Zhao, and S. Liu, "A dual-input high step-Up DC/DC converter With ZVT auxiliary circuit," *IEEE Trans. Energy Convers.*, vol. 34, no. 1, pp. 161–169, Mar. 2019.

[10] F. Yang, H. Ge, J. Yang, and H. Wu, "Dual-input grid-connected photovoltaic inverter with two integrated DC–DC converters and reduced conversion stages," *IEEE Trans. Energy Convers.*, vol. 34, no. 1, pp. 292–301, Mar. 2019.

[11] M. Azizi, M. Mohamadian, and R. Beiranvand, "A new family of multi-input converters based on three switches leg," *IEEE Trans. Ind. Electron.*, vol. 63, no. 11, pp. 6812–6822, Nov. 2016.

[12] J. Zhang, H. Wu, X. Qin, and Y. Xing, "PWM plus secondary-side phase-shift controlled soft-switching full-bridge three-port converter for renewable power systems," *IEEE Trans. Ind. Electron.*, vol. 62, no. 11, pp. 7061–7072, Nov. 2015.

[13] S. Khosrogorji, M. Ahmadian, H. Torkaman, and S. Soori, "Multi-input DC/DC converters in connection with distributed generation units—A review," *Renew. Sust. Energy Rev.*, vol. 66, pp. 360–379, Dec. 2016.

[14] H. Zhu, D. Zhang, Q. Liu, and Z. Zhou, "Three-Port DC/DC converter with all ports current ripple cancellation using integrated magnetic technique," *IEEE Trans. Power Electron.*, vol. 31, no. 3, pp. 2174–2186, Mar. 2016.

[15] A. Deihimi, M. E. Seyed Mahmoodieh, and R. Iravani, "A new multi-input step-up DC–DC converter for hybrid energy systems," *Elec. Power Syst. Res.*, vol. 149, pp. 111–124, Aug. 2017.

[16] Y. M. Chen, Y. C. Liu, S. C. Hung, and C. S. Cheng, "Multi-Input Inverter for Grid-Connected Hybrid PV/Wind Power System," *IEEE Trans. Power Electron.*, vol. 22, no. 3, pp. 1070–1077, May 2007.

[17] S. Bae and A. Kwasinski, "Dynamic modeling and operation strategy for a microgrid with wind and photovoltaic resources," *IEEE Trans. Smart Grid*, vol. 3, no. 4, pp. 1867–1876, Dec. 2012.

[18] L. Wang, Q. H. Wu, and W. Tang, "Novel cascaded switched-diode multilevel inverter for renewable energy integration," *IEEE Trans. Energy Convers.*, vol. 32, no. 4, pp. 1574–1582, Dec. 2017.

[19] N. K. Reddi, M. R. Ramteke, H. M. Suryawanshi, K. Kothapalli, and S. P. Gawande, "An isolated multi-input ZCS DC–DC front-end-converter based multilevel inverter for the integration of renewable energy sources," *IEEE Trans. Ind. Appl.*, vol. 54, no. 1, pp. 494–504, Jan./Feb. 2018.

[20] B. Mangu, S. Akshatha, D. Suryanarayana, and B. G. Fernandes, "Grid-connected PV-wind-battery-based multi-input transformer-coupled bidirectional DC-DC converter for household applications," *IEEE J. Emerg. Sel. Topics Power Electron.*, vol. 4, no. 3, pp. 1086–1095, Sep. 2016.

[21] P. C. Loh, L. Zhang, and F. Gao, "Compact integrated energy systems for distributed generation," *IEEE Trans. Ind. Electron.*, vol. 60, no. 4, pp. 1492–1502, Apr. 2013.

[22] X. Liu, P. C. Loh, P. Wang, and F. Blaabjerg, "A Direct Power Conversion Topology for Grid Integration of Hybrid AC/DC Energy Resources," *IEEE Trans. Ind. Electron.*, vol. 60, no. 12, pp. 5696–5707, Dec. 2013.

[23] W. Jiang and B. Fahimi, "Multiport power electronic interfaceâĂŤConcept, modeling, and desig," *IEEE Trans. Power Electron.*, vol. 26, no. 7, pp. 1890–1900, Jul. 2011.

[24] P. Shamsi and B. Fahimi, "Dynamic behavior of multiport power electronic interface under source/load disturbances," *IEEE Trans. Ind. Electron.*, vol. 60, no. 10, pp. 4500–4511, Oct. 2013.

[25] H. Bizhani, R. Noroozian, S. M. Muyeen, and F. Blaabjerg, "Wind farm grid integration architecture using unified expandable power converter," *IEEE Trans. Power Electron.*, vol. 34, no. 4, pp. 3407–3417, Apr. 2019.

[26] Z. Qin, P. C. Loh, and F. Blaabjerg, "Application criteria for nine-switch power conversion systems with improved thermal performance," *IEEE Trans. Power Electron.*, vol. 30, no. 8, pp. 4608–4620, Aug. 2015.

[27] H. Bizhani, G. Yao, S. M. Muyeen, S. M. Islam, and L. B. Brahim, "Dual mechanical port machine based hybrid electric vehicle using reduced switch converters," *IEEE Access*, vol. 7, pp. 33665–33676, 2019.

[28] S. M. Muyeen, R. Takahashi, T. Murata, and J. Tamura, "A variable speed wind turbine control strategy to meet wind farm grid code requirements," *IEEE Trans. Power Syst.*, vol. 25, no. 1, pp. 331–340, Feb. 2010.

HAMED BIZHANI (S'17) was born in Mashhad, Iran, in 1988. He received the B.Sc. degree in electrical engineering from Birjand University, Birjand, Iran, in 2011, and the M.Sc. degree in electrical engineering from the K. N. Toosi University of Technology, Tehran, Iran, in 2013. He is currently pursuing the Ph.D. degree in electrical engineering with the University of Zanjan, Zanjan, Iran. He was a Visiting Research Associate with Curtin University, Perth, Australia. His current research interests include multiport power electronic converters, the control and integration of distributed generations, space vector modulation, and hybrid electric vehicle.

REZA NOROOZIAN (M'09) was born in Iran. He received the B.Sc. degree from the University of Tabriz, Tabriz, Iran, in 2000, and the M.Sc. and Ph.D. degrees in electrical engineering from the Amirkabir University of Technology, Tehran, Iran, in 2003 and 2008, respectively. He is currently a Professor with the Department of Power Engineering, University of Zanjan, Zanjan, Iran. His reserach interests include power electronics, power systems, power quality, the integration and control of renewable generation units, custom power, micro grid operation, distributed-generation modeling, and operation and interface control.

S. M. MUYEEN (S'03–M'08–SM'12) received the B.Sc.Eng. degree from the Rajshahi University of Engineering and Technology (RUET), Bangladesh, in 2000, and the M.Eng. and Ph.D. degrees from the Kitami Institute of Technology, Japan, in 2005 and 2008, respectively, all in electrical and electronic engineering. He is currently an Associate Professor with the Department of Electrical and Computer Engineering, Curtin University, Perth, Australia. He has published more than 200 articles in different journals and international conferences. He has published six books as an author or editor. His research interests include power system stability and control, electrical machine, FACTS, energy storage systems (ESS), renewable energy, and HVDC systems. He is a Fellow of Engineers Australia. He is serving as an Editor/Associate Editor for many prestigious Journals from IEEE, IET, and other publishers including the IEEE TRANSACTIONS OF SUSTAINABLE ENERGY, the IEEE POWER ENGINEERING LETTERS, *IET Renewable Power Generation*, and *IET Generation, Transmission and Distribution*. He has been a Keynote Speaker and an Invited Speaker at many international conferences, workshops, and universities.

KUAANAN TECHATO received the B.Eng. degree in ME from the Prince of Songkla University, Thailand, in 1995, the M.Eng. degree in IE from Chulalongkorn University, in 1999, the M.Sc. degree in EBM from Warwick University, in 1999, and the Ph.D. degree from Chulalongkorn University, in 2008. He is currently an Assistant Professor with the Prince of Songkla University, Hadyai Campus, Thailand, where he is also serving as the Dean of the Faculty of Environmental Management. His research interests include renewable energy, heat-pump, and power system and control. He has been a Keynote Speaker and an Invited Speaker at many international conferences. He has published many technical articles to various journals and international conferences. He is also involved with many Journals as an Editor or an Associate Editor and a successful organizer for many international conferences.

FREDE BLAABJERG (S'86–M'88–SM'97–F'03) received the Ph.D. degree in electrical engineering from Aalborg University, in 1995. He became an Assistant Professor, in 1992, an Associate Professor, in 1996, and a Full Professor of power electronics and drives, in 1998. He was with ABB-Scandia, Randers, Denmark, from 1987 to 1988. In 2017, he became a Villum Investigator. He has published more than 500 journal papers in the fields of power electronics and its applications. He has coauthored two monographs and editor of seven books in power electronics and its applications. His current research interests include power electronics and its applications such as in wind turbines, PV systems, reliability, harmonics, and adjustable speed drives. He has received 26 IEEE Prize Paper Awards, the IEEE PELS Distinguished Service Award, in 2009, the EPE-PEMC Council Award, in 2010, the IEEE William E. Newell Power Electronics Award 2014, and the Villum Kann Rasmussen Research Award 2014. He received the Honoris Causa from University Politehnica Timisoara (UPT), Romania, and Tallinn Technical University (TTU), Estonia. He was the Editor-in-Chief of the IEEE TRANSACTIONS ON POWER ELECTRONICS, from 2006 to 2012. He has been a Distinguished Lecturer for the IEEE Power Electronics Society, from 2005 to 2007 and for the IEEE Industry Applications Society, from 2010 to 2011 and 2017 to 2018. In 2018, he was the President Elect of the IEEE Power Electronics Society. He is nominated in 2014, 2015, 2016, and 2017 by Thomson Reuters to be between the most 250 cited researchers in Engineering in the world.

• • •